

Ligand-Binding Pocket Shape Differences between Sphingosine 1-Phosphate (S1P) Receptors S1P₁ and S1P₃ Determine Efficiency of Chemical Probe Identification by Ultrahigh-Throughput Screening

Stephan C. Schürer^{†,‡}, Steven J. Brown^{§,‡}, Pedro J. Gonzalez-Cabrera[¶], Marie-Therese Schaeffer[§], Jacqueline Chapman[§], Euijung Jo[¶], Peter Chase[§], Tim Spicer[§], Peter Hodder[§], and Hugh Rosen^{¶,*}

[†]Department of Scientific Computing, [§]The Scripps Research Institute Molecular Screening Center, and [¶]Department of Chemical Physiology, The Scripps Research Institute, La Jolla, California and Jupiter, Florida, [‡]These authors contributed equally to this work.

ABSTRACT We have studied the sphingosine 1-phosphate (S1P) receptor system to better understand why certain molecular targets within a closely related family are much more tractable when identifying compelling chemical leads. Five medically important G-protein-coupled receptors for S1P regulate heart rate, coronary artery caliber, endothelial barrier integrity, and lymphocyte trafficking. Selective S1P receptor agonist probes would be of great utility to study receptor subtype-specific function. Through systematic screening of the same libraries, we identified novel selective agonist chemotypes for each of the S1P₁ and S1P₃ receptors. Ultrahigh-throughput screening (uHTS) for S1P₁ was more effective than that for S1P₃, with many selective, low nanomolar hits of proven mechanism emerging. Receptor structure modeling and ligand docking reveal differences between the receptor binding pockets, which are the basis for subtype selectivity. Novel selective agonists interact primarily in the hydrophobic pocket of the receptor in the absence of headgroup interactions. Chemistry-space and shape-based analysis of the screening libraries in combination with the binding models explain the observed differential hit rates and enhanced efficiency for lead discovery for S1P₁ versus S1P₃ in this closely related receptor family.

*Corresponding author,
hrosen@scripps.edu.

Received for review March 6, 2008
and accepted June 5, 2008.

Published online July 1, 2008

10.1021/cb800051m CCC: \$40.75

© 2008 American Chemical Society

Sphingosine 1-phosphate (S1P, **1**, Supplementary Figure S1) mediates a wide variety of physiological responses, including heart rate (*1, 2*), coronary artery caliber, endothelial integrity, and lymphocyte recirculation (*1, 3–5*) through high-affinity interactions with five members of the endothelial differentiation gene (EDG) family of plasma membrane-localized G-protein-coupled receptors (GPCRs), the sphingosine lipid receptors, S1P_{1–5} (*6–8*). Inhibition of lymphocyte recirculation by nonselective S1P receptor agonist FTY720 (**2**, Supplementary Figure S1) produces clinical immunosuppression in multiple sclerosis. This prodrug, once phosphorylated by sphingosine kinase 2, acts as a potent agonist at S1P₁, S1P₃, S1P₄, and S1P₅ (*9*). S1P₁ is associated with immunosuppression, while other subtypes contribute to dose-limiting mechanism-based bradycardia and bronchoconstriction. Understanding the contribution of individual receptors has been limited by the unavailability of selective agonists or antagonists for the five receptor subtypes. Selective probes of receptor function synergize with genetic models and allow validation of new therapeutic targets that are chemically tractable (*10*). S1P receptor subtype selective agonists and antagonists will be of broad utility in understanding cell functions *in vitro*, and vascular physiology *in vivo*. Success of the chemical approach for S1P₁ suggests that developing selective tools for the resolution of function across this broad lipid receptor family is now possible (*23–13*). SEW2871 (**3**, Supplementary Figure S1) is an *in vivo* active heterocyclic selective S1P₁ agonist probe originally identified by high-

throughput screening (HTS) (1). SEW2871 unlike FTY720 recapitulates the action of S1P and demonstrates the essential role of the S1P₁ receptor in lymphocyte trafficking (4). The development of pharmacophore models of receptor subtype-selective agonist and antagonist interactions would aid rational design and lead optimization, which is still severely limited by the lack of selective agonists for S1P₂, S1P₃, S1P₄, and S1P₅ subtypes. The S1P receptors belong to the largest subfamily A of GPCRs for which high-resolution X-ray structures are available (14, 15). Homology models of the S1P₁ and S1P₄ receptors based on a theoretical rhodopsin model and mutagenesis studies have identified three key polar headgroup interactions of S1P with its receptors (16, 17). The S1P₁ and S1P₃ receptors are the most closely related members of this family with about 50% identical and >70% similar amino acids (18). Key residues that constitute the hydrophobic binding pocket of the S1P₁ and the S1P₃ receptors have been identified (19).

Here we report novel S1P₁ and S1P₃ agonist series identified by HTS. Despite the high homology between these sphingolipid receptors, the confirmed hit rate was much higher for S1P₁ than S1P₃. Mapping of the hit series onto diversity space demonstrates that S1P₁ ligands are better represented in the screening collections. Homology modeling of the S1P₁ and S1P₃ receptors and induced fit docking studies of the receptor binding interaction of the selective S1P₁ and S1P₃ agonist series reveal, in part, the basis for S1P₁ versus S1P₃ agonist specificity. SAR analysis and comparison of the binding modes of the new agonist series and the natural S1P ligand indicate their primary interaction with the hydrophobic binding pocket.

RESULTS AND DISCUSSION

S1P₁ and S1P₃ Ultrahigh-Throughput Screening (uHTS) and Confirmation. In order to identify novel and specific entry points for agonists of the S1P₁ and S1P₃ receptors, we developed CRE (S1P₁) and NFAT (S1P₃, coupled *via* the promiscuous G-protein α 16) promoter β -lactamase reporter cell lines and used these to construct robust HTS assays (20). We examined the structural diversity of the Molecular Libraries Small Molecule Repository (MLSMR) and the Maybridge HitFinder (MBHF) collection using a chemistry-space- and fingerprint-based method; the libraries are sufficiently diverse from one another (see Methods and Supple-

mentary Figures S2 and S3), and we therefore screened both libraries in an effort to identify unique lead series.

The MBHF and MLSMR libraries were screened in 384 and 1536 well formats, respectively. With the S1P₁ cell line, two closely related screens were conducted, one for agonists and the second designed to identify potentiators of S1P₁ agonists. Thus we used the data from both assays to identify compounds that reproducibly act as S1P₁ agonists. Active wells in the primary screening assay were confirmed and counterscreened against the parental cell line to eliminate compounds activating the reporter nonspecifically. The S1P₃ actives were counterscreened against the 5HT1A/G α 16/NFAT-bla CHO-K1 cell line expressing the 5HT1A serotonin receptor subtype, because it is highly unlikely that a true S1P₃ agonist compound would also have a high affinity for this receptor. Any S1P₁ or S1P₃ active compounds also active in the respective counterscreening assay were considered nonspecific and of no further interest. The majority of false positive compounds fall into one of two classes. First, blue fluorescent and green fluorescence quenching compounds modify the 410 nm excitation/460 nm emission (blue) to 410 nm excitation/590 nm emission intensity (green) ratio of the CCF4 FRET dye such that they appear to be agonists. The second class of compounds activates the promoter for the reporter assay nonspecifically. In either case, activity in the counterscreening assays are used to exclude such hits. Screening statistics and confirmation numbers are summarized in Supplementary Table S1. Dose response curves were measured using solid compound of confirmed structure for selected higher potency compounds.

Initial structure–activity results were independently hierarchically clustered using Leadscape keys (21). Chemical series and individual compounds with activity in the parental cell lines and reactive or chemically undesired motifs were removed. The statistical characterization of the most active structural series as identified by the initial concentration–response confirmation assay for the two receptors are shown in Supplementary Table S2. A series of 3,5-diaryl-oxadiazole (represented by structure **5**, Supplementary Table S2) is the largest and highest scoring analog series of S1P₁ agonists with selectivity against S1P₃. Although of lower potency compared with S1P₁, a subset of the 3,5-diaryl-oxadiazoles also forms one of the most active clusters

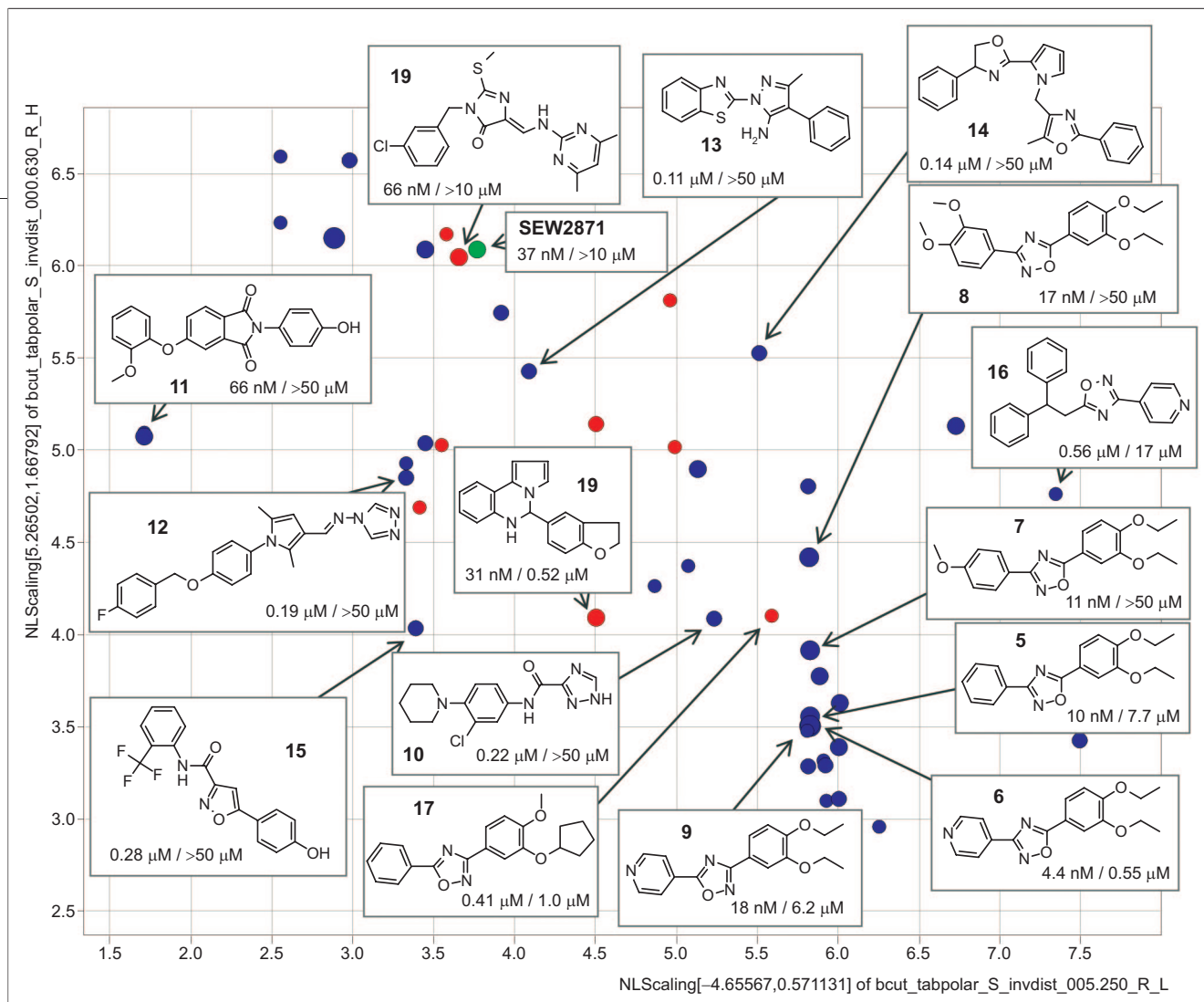


Figure 1. Representative S1P₁ agonists with EC₅₀ < 1 μM in a two-dimensional chemistry space. EC₅₀ values are shown for S1P₁/S1P₃ (blue MLSMR, red MBHF, green SEW2871; size is scaled by S1P₁ pEC₅₀).

of S1P₃ agonists; this is because of the overall much lower potency of identified S1P₃ versus S1P₁ agonists.

To extend the SAR of the S1P₁ agonists, we built similarity clusters around the most active compounds (S1P₁ EC₅₀ < 1 μM) and removed redundancy by hierarchical clustering using Leadscape keys. This method also brings back compounds that were inactive in the primary screen.

Potencies (confirmed from fresh samples), source, and diversity (using a two-dimensional BCUTS chemistry space) of identified S1P₁ agonists with an EC₅₀ of less than 1 μM are illustrated in Figure 1. Structures of various scaffolds are exemplified including the most privileged cluster of 3,5-diaryl-oxadiazoles, among them the most active and selective 3-(4-pyridyl)-5-(3,4-diethoxyphenyl)-1,2,4-oxadiazole (**6**) with an EC₅₀ of 4 nM. SAR of the oxadiazole series in the context of the receptor binding model is discussed below (Table 1). Representative S1P₁ agonists of the confirmed series are also shown in Supplementary Table

S3; additional actives identified from the Maybridge library are shown in Supplementary Table S4.

Potency, diversity, and source of S1P₃ agonists are illustrated in Figure 2. Interestingly the prevalence of confirmed hits for S1P₃ identified from the Hitfinder library compared with the MLSMR library was the opposite of that seen for S1P₁. Because of the generally higher diversity of this collection compared with the MLSMR library only singletons and no structural series were identified; their activities and confirmatory calcium flux assay results are provided in Supplementary Table S5. The examples include novel nanomolar agonists with selectivity against S1P₁ and confirmed mechanism of action. To our knowledge, there are currently no selective S1P₃ agonists. The most active oxadiazole S1P₁ agonist identified from the MLSMR library also is among the most—although much less—active S1P₃ agonists. From the MLSMR library, we identified dicyclohexylamide **20** as a nanomolar selective S1P₃ agonist (S1P₃ EC₅₀ = 0.35 μM, S1P₁ EC₅₀ > 10 μM and inactive

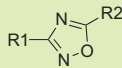
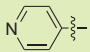
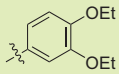
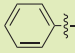
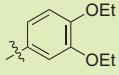
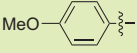
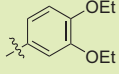
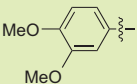
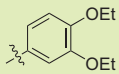
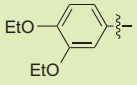
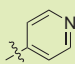
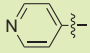
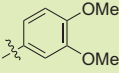
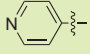
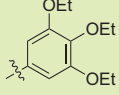
against S1P₂, S1P₄, S1P₅, LPA₁, LPA₂, and LPA₃ (Supplementary Table S6). Its 5-methyl derivative, also a S1P₃ screening hit, (not shown) is significantly less active (~11 μM).

Secondary Assay Confirmation and Subtype

Selectivity of Lead Series. Agonist-mediated internalization and lysosomal degradation of the S1P₁ receptor by AFD-R (**4**, Supplementary Figure S1), the native ligand S1P (**1**), and SEW2871 (**3**) occurs with a 3 log concentration differential (AFD-R ≫ S1P > SEW2871) (22). Like other S1P agonists, stimulation with the novel agonist **6** (Figure 1, Table 1) causes S1P₁-eGFP internalization, protein phosphorylation, and polyubiquitination. Thus, **6** is a compound with full agonist potential, clearly differentiated in biological potential from the oft-utilized S1P₁ probe of moderate potency, SEW2871. Agonist-stimulated receptor phosphorylation was studied using GFP immunoprecipitates in S1P₁-GFP stable cells that were metabolically labeled with ³²P prior to agonist incubation. The same immunoprecipitation protocol has been successfully used to report receptor degradation pathways (22). Accordingly, the EC₅₀ for S1P-mediated receptor phosphorylation (at 30 min of incubation) was determined to be 5 nM (not shown). Figure 3 shows that incubation of agonists for 30 min resulted in ³²P incorporation into the immunoprecipitated receptor, with AFD-R being more efficacious (eliciting the greatest response) relative to S1P or the selective S1P₁ agonist **6**. S1P₃ activation by the agonist **20** (Figures 2 and 4) and a subsequent follow-up analog **28** (Figure 4) induced calcium flux to the same extent as S1P (Figure 3 panel C). Compounds **6** and **20** were also tested against S1P₂, S1P₄, S1P₅, LPA₁, LPA₂, and LPA₃ and show exquisite selectivity: oxadiazole **6** with an EC₅₀ for S1P₁ of 5 nM and EC₅₀ for S1P₃ of 0.5 μM is inactive against the other S1P receptors and LPA₁₋₃; dicyclohexylamide **20** with an EC₅₀ for S1P₃ of 350 nM is inactive for all other S1P receptors and LPA₁₋₃. Thus we have identified biologically active compounds, specific for either receptor, from uHTS.

S1P₁ and S1P₃ Receptor Binding Models. The striking difference between the number and potency of confirmed agonists identified in the S1P₁ and S1P₃ campaigns led us to evaluate the receptor binding models. Among the sphingosine lipid receptors, S1P₁ and S1P₃ are the most closely related by sequence. Their agonist binding pockets, which consist of an upper polar region (16, 17) and a lower hydrophobic pocket (18, 19), are

TABLE 1. SAR of Selected 3,5-Diaryloxadiazoles^a

				
R1	R2		EC ₅₀ S1P ₁	EC ₅₀ S1P ₃
		6	4.4	550
		5	10	7700
		7	11	>50K
		8	17	>50K
		9	18	6200
		29	135	>50K
		30	>50K	>50K

^aEC₅₀ reported in nM.

even more similar. Yet there is a remarkable difference in small molecule agonist recognition, as demonstrated by the different confirmed hit rates for the HTS campaigns. The development of a structural hypothesis underlying these differences has been limited by the lack of experimental structures of any of the receptors, and homology modeling can be a valuable approach to develop structural insight in these receptors (16–19). Our first step therefore was to develop two comparable mod-

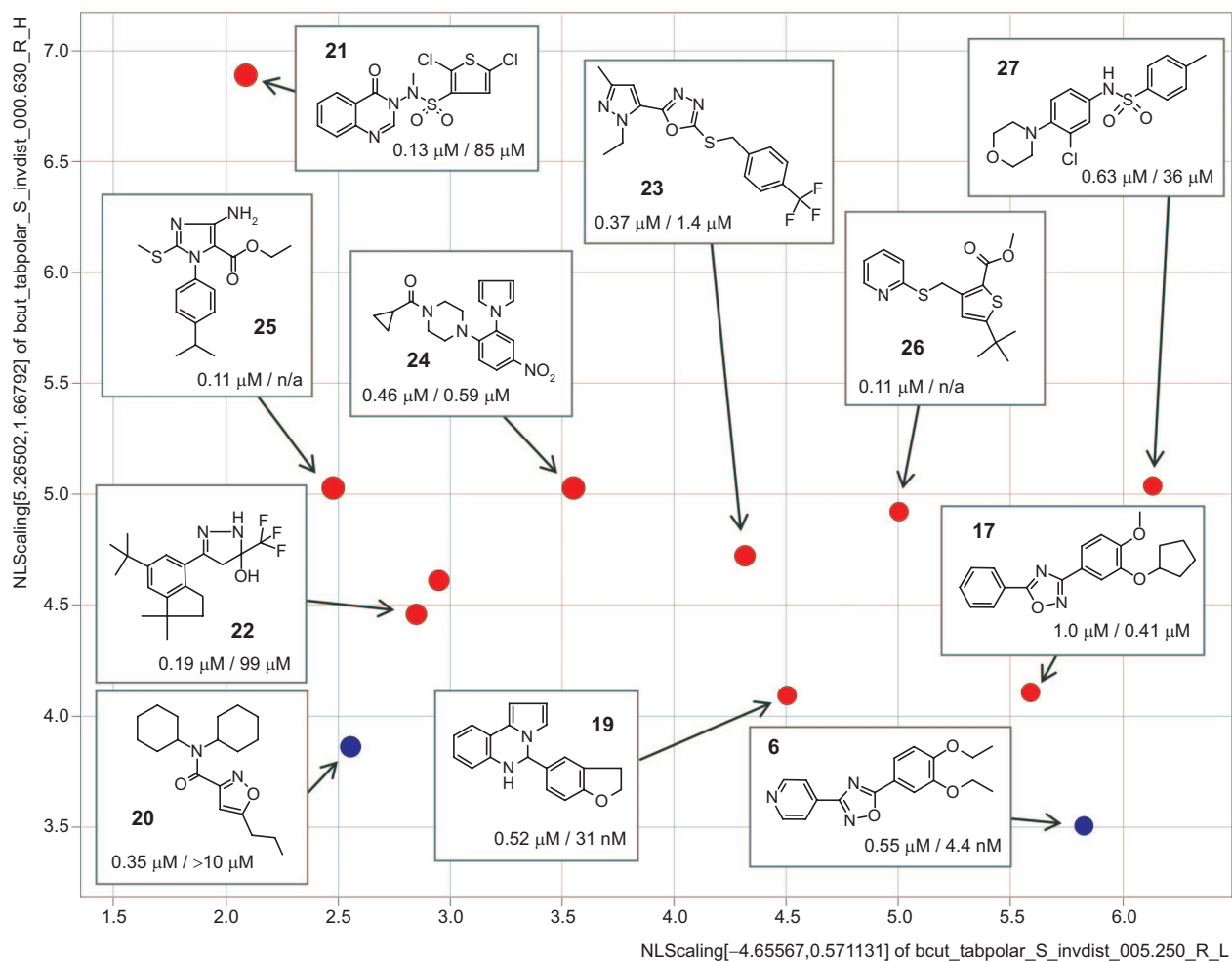


Figure 2. S1P₃ agonists with EC₅₀ < 1 μM in a two-dimensional chemistry space. EC₅₀ values are shown for S1P₃/S1P₁ (blue MLSMR, red MBHF; size is scaled by S1P₃ pEC₅₀).

els of the S1P₁ and S1P₃ receptors. The initial homology model of S1P₁ was built based on a high-resolution crystal structure of chain A of bovine rhodopsin (PDB 1u19, 2.2 Å resolution) (15) with retinal in the unactivated (cis) conformation, which was refined involving repositioning the second extracellular loop connecting TM4 and TM5, local and global minimizations, and side chain optimization of the hydrophobic part of the pocket using induced fit docking (IFD) (23) runs with S1P and FTY720-P as known ligands as described in Methods. The final S1P₁ model was then used as a template to build the corresponding S1P₃ model. Although the

ceptor side chain positions may vary depending on the specific receptor–ligand complex our goal was to minimize modeling bias and develop structures that are exactly aligned and in which the binding pockets can therefore be directly compared. We also generated models based on a more recent structure of lumirhodopsin (PDB 2hpy, 2.8 Å resolution) (24), a photoactivated all-trans retinal intermediate of the activated receptor (See Methods). For all docking studies, we used the optimized structures based on the higher resolution “dark-state” rhodopsin, modeling a prospective snapshot of ligand binding prior to receptor activation.

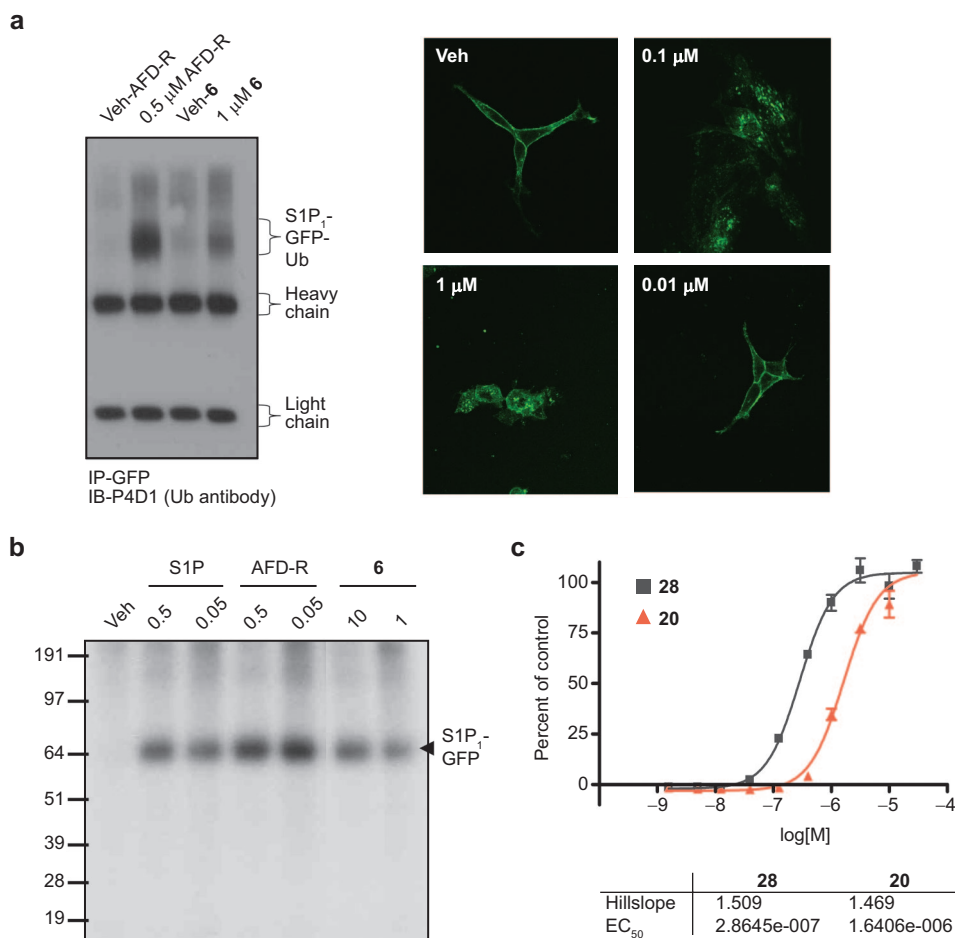


Figure 3. Biological activity of S1P₁ and S1P₃ agonists. a) S1P₁–GFP internalization and ubiquitination by 6. b) Agonist-induced ³²P incorporation into immunoprecipitated S1P₁–GFP. c) S1P₃ agonist dose-dependent activation of calcium flux in S1P₃/ga16 CHO cells by 20 and 28.

Our models suggest that one of the major differences of the binding pockets is determined by Leu276 in S1P₁ versus Phe263 in S1P₃ as illustrated by the surface representation of both receptors with the S1P and FTY720-P agonists docked into the pocket (Figure 5). The Phe263 residue results in a contraction of the pocket between the lower hydrophobic pocket and the upper polar section by 1.5–1.8 Å compared with the corresponding S1P₁ Leu276 residue; this also results in a difference in binding pocket volume between 50 and 100 Å³ (see Methods). Additional illustrations of the S1P₁ and S1P₃ receptor binding sites with docked S1P and FTY720-P and illustrations of their detailed binding interactions in the receptor models are provided in Supplementary Fig-

ures S4 and S5. The difference in spatial constraint between the polar and hydrophobic sections of the binding pockets of S1P₁ and S1P₃ may explain the lower frequency and potency of S1P₃ versus S1P₁ agonists (vide infra); presumably the S1P₁ pocket may accommodate more rigid and perhaps larger ligands compared with S1P₃.

Compared with an available model of S1P₁ (25) the seven transmembrane domains are overall well-aligned with our models but with some of the active site residues in a different orientation. The largest variation is in the position of the second extracellular loop, which would interfere with S1P binding. Recently a study comparing models of all five S1P receptors in the context of

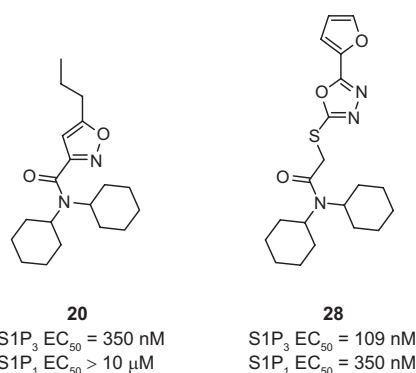


Figure 4. Structure and activity of $S1P_3$ selective dicyclohexylamides **20** and **28**.

known modulators including S1P, FTY720-P, and SEW2871 was published (26). The described key residues involved in recognition of S1P and FTY720-P indicate that our models are largely in agreement although this study does not refer to the influence of Leu276 versus Phe263. The main difference between $S1P_1$ and $S1P_3$ was described as the length of the binding pocket and illustrated in the docked conformations of S1P and FTY720-P; our models are different in that respect as a result of the modeling process. Our models seem in best agreement with the studies by Parent *et al.* (18) who also identify the Leu276 and Phe263 as a key determinant of the $S1P_1/S1P_3$ selectivity. Structure models

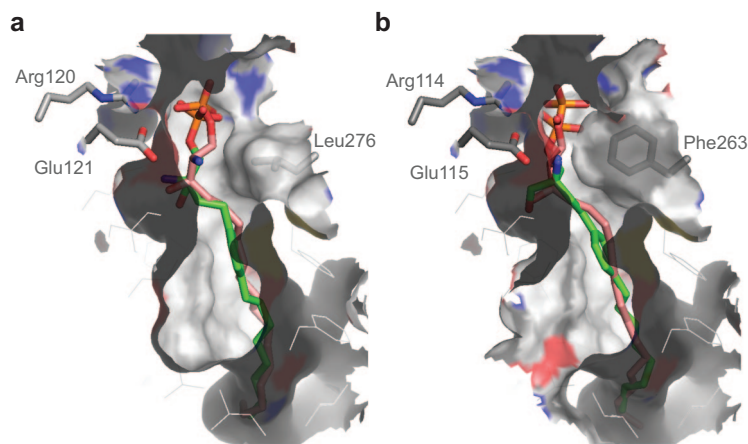


Figure 5. Comparison of the binding pocket of the $S1P_1$ (a) and $S1P_3$ (b) receptors with S1P and FTY720-P docked into each receptor. The main difference in the binding pocket derives from the $S1P_1$ Leu276 and $S1P_3$ Phe263 side chains; in $S1P_3$, the binding pocket is narrowed by 1.5–2 Å compared with the same region in $S1P_1$.

based on templates of only remote (<20%) homology such as ours and other reported S1P receptor structures clearly can be useful to suggest pharmacological trends; however, their absolute accuracy remains unknown, and they are therefore most effectively applied in the context of experimental data.

Binding Hypothesis of Selective Agonists for $S1P_1$ and $S1P_3$. Examples of the 3,5-diaryl-oxadiazole series of selective $S1P_1$ agonists are given in Table 1 to illustrate the influence of hydrophobic space and positioning of the two aryl moieties.

The four most active compounds were docked, aligned, and minimized in the receptor site as described in Methods (Figure 6). An overlay of the four structures in the receptor is shown in the Supplementary Figure S6.

In our models, the diethoxyphenyl moieties reach down into the hydrophobic part of the pocket with the pyridyl or phenyl substituents reaching toward the upper, more polar portion of the pocket between Glu121 and Leu276. In this orientation, the top aryl moiety interferes with Phe263 of $S1P_3$, which can rationalize the observed selectivity (Figure 6). Oxadiazoles with spatially more demanding substituents 4-methylphenyl and 3,4-dimethylphenyl are less potent against $S1P_1$ but become completely inactive for $S1P_3$. This spatially more constrained section of the $S1P_3$ binding pocket may have a larger effect as the size of the interacting substituent increases. The higher activity of the pyridine- (**6**) versus phenyl-substituted compound (**5**) may relate to the more polar environment of this part of the pocket, although the distance of the pyridine N and Arg120 NH (3.7 Å) seems too large for a direct hydrogen bond and an interaction with Glu121 is not expected at neutral pH unless a water molecule participates. In all ligands, the aromatic ring systems are slightly out of plane and not in their optimal geometric (all planar) conformation, particularly the 3-substituent that reaches up toward the more polar region of the binding site. The most active compounds all share the hydrophobic 2,3-diethoxyphenyl moiety. Introduction of an additional ethoxy substituent results in loss of activity (compare **6** and **30**). This is explained given the binding model in Figure 5, which indicates interference of any additional substituent on the phenyl with Trp269 and Phe273 of TM6. A smaller group, 2,3-dimethoxy-phenyl versus 2,3-diethoxy-phenyl (**6** vs **29**) results in decreased activity (30-fold), probably due to less effective interaction with

hydrophobic residues required for receptor activation. Reversing the orientation of the oxadiazole (*i.e.*, swapping the 3 and 5 substituents as in **6** vs **9**) results in decreased activity for both receptors. A previous study reports activity of different five-membered heterocycles against S1P₁, S1P₃, and S1P₅ (27). Although their compounds all include a carboxylic acid headgroup presumably interacting with one or more of the arginine side chains, the authors report a decrease in S1P₁ activity when the 3,5-1,2,4-oxadiazole is replaced, for example, with a 2,5-1,3,4-oxadiazole core in otherwise identical structures. In our homology model, Cys200 can be oriented to form a hydrogen bond with the oxadiazole oxygen (S–O distance \approx 2.2 Å), a potential explanation for this observed effect (not shown).

From the MLSMR library, we identified the nanomolar S1P₃ selective agonist **20** (Figure 4). Based on the hypothesis that the dicyclohexylamide would interact in the hydrophobic binding pocket of S1P₃, we tested additional commercial analogs, one of which, **28**, was found to be even more active (but less selective). Docking of these ligands confirms this possible binding mode (Figure 7). The propyl-isoxazole moiety of the relatively compact **20** warps underneath and slightly behind Phe263. Similarly, the furanyl moiety of **28** avoids the contraction of the S1P₃ binding pocket. The overlaid structures in the receptor are shown in the Supplementary Figure S7. Interestingly, the docked structures in Figure 7 do interfere with Leu276 of S1P₁, which may explain their selectivity. A possible orientation of **28**, which is only three times selective over S1P₁, in the S1P₁ receptor is illustrated in Supplementary Figure S9 (see Methods).

When the poses of the selective diaryloxadiazole S1P₁ and the above S1P₃ agonists are compared, the respective diethoxyphenyl and dicyclohexylamide moieties reaching into the hydrophobic pocket align reasonably with respect to shape. Our structural models and docking poses suggest that the moieties reaching toward the polar region at least in part determine selectivity. In the case of S1P₁, the relatively rigid diaryloxadiazoles occupy space between Glu121 and Leu276 with the plane of the upper 3-aryl moiety aligned between the TM3 and TM6 domains. The potent and selective S1P₃ agonists are less spatially demanding in that region and more flexible to adopt a conformation in which this “upper” ligand moiety can adapt to the spatial constraint of the pocket imposed by Phe263. In the

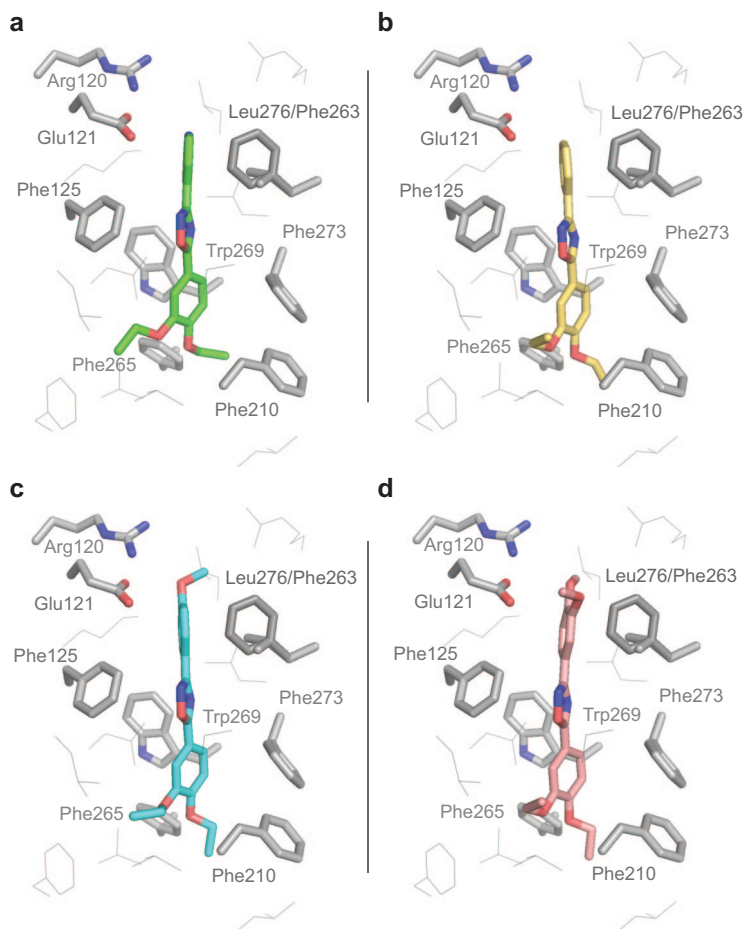


Figure 6. Oxadiazoles docked into the S1P₁ receptor: **6**, green (a); **5**, yellow (b); **7**, cyan (c); **8**, copper (d). The S1P₃ Phe263 residue interferes with these ligand poses explaining the observed selectivity.

case of **28**, the orientation of the plane of the furanyloxadiazole in S1P₃ is almost perpendicular to the one of the 3-aryl plane of the oxadiazoles in S1P₁. In the pose of **28** in S1P₁, these aryl moieties align parallel.

As described above, computer-generated models of the S1P₁ and S1P₃ receptor ligand binding pockets differ most strikingly with Leu276 of S1P₁ replaced with Phe263 of S1P₃ (18). Docking of the S1P₃-specific compound **20** into the S1P₁ model is influenced by the proximity of Leu276 and generates poses with less favorable docking scores. In order to evaluate the validity of the S1P₁ modeling, we generated the S1P₁ L276F mutation and measured extracellular-regulated kinase (ERK) phosphorylation in response to S1P and the S1P₃ spe-

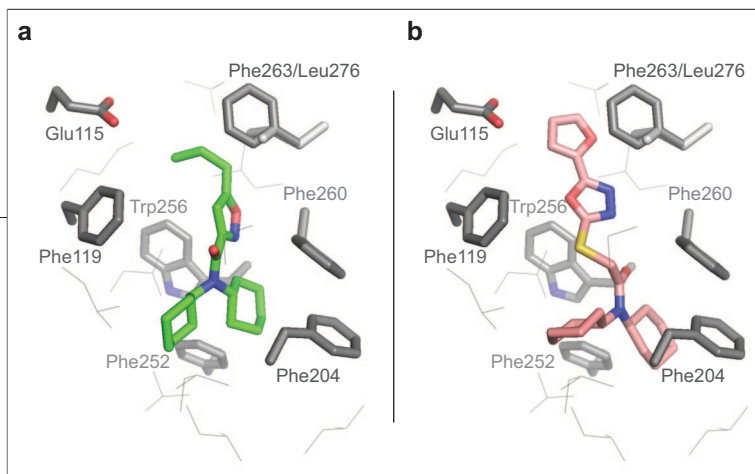


Figure 7. S1P₃-selective dicyclohexylamides docked into the S1P₃ receptor hydrophobic binding pocket: green, **20** (a); copper, **28** (b).

cific compound **20**. Indeed, **20**, while inactive at 30 μ M on wild-type S1P₁ elicits a striking pERK response (EC_{50} 1.4 μ M) in the L276F mutant (Supplementary Figure S12). Thus the S1P₁ L276F mutation results in a gain of function with the S1P₃-selective compound **20**.

Ligand Shape Confers Receptor Specificity. Our results suggest that the more linear and rigid aromatic diaryloxadiazole ligands fit the S1P₁ pocket while the more compact flexible dicyclohexylamide derivatives prefer S1P₃. Mutations of residues lining the ligand binding pocket to smaller side chains frequently lead to loss of receptor activation by S1P (19). The S1P₁ and by extension the highly related S1P₃ receptors are only activated by ligands of sufficient volume to interact in the hydrophobic pocket of the receptors. Our models and docking studies suggest that in contrast to any of the known S1P₁ agonists, both of our selective S1P receptor agonist series have no obvious interaction with any of the glutamate (Glu121) or arginine (Arg120; Arg292) residues that form their well-established polar binding sites and, in this respect, constitute ligands with a novel binding mode. This hypothesis is now experimentally confirmed by mutation studies and further analogs of **6** (manuscript in preparation). Our S1P receptor agonists interact in the lower hydrophobic binding pocket, while their selectivity can be rationalized by the receptor-specific ligand conformations matching the spatial requirements toward the upper section of the binding pocket.

Conclusion and Potential for Discovery of Selective Agonists. In contrast to S1P₁, fewer and less potent agonists were identified for S1P₃. It can be qualitatively expected that a binding pocket that is spatially constrained in one area may have fewer potential ligands, which on average may interact with lower potency because conformational flexibility and ligand size relate to binding energy. However the relative confirmed hit rates are a function of the screening library composition. To quantify this effect, we compared the shape of the

docked conformations of the most active and selective agonists for S1P₁ and S1P₃ against the entire MLSMR and MBHF screening library. The results are illustrated in Supplementary Figure S10 and confirm that there are many more shape-similar compounds for the S1P₁ diaryloxadiazole agonist **6** compared with the dicyclohexylamide **20**. This reflects the composition of typical screening libraries relative to the identified selective S1P₁ and S1P₃ agonists **6** and **20** in their preferred docked conformations. An analysis of the density of the chemistry space that characterizes the MLSMR and MBHF libraries shows that the majority of the identified S1P₁ agonists fall into higher occupied regions compared with the S1P₃ agonists (Supplementary Figure S11). This is a receptor structure independent perspective also suggesting screening library bias toward S1P₁ versus S1P₃.

Summary. Selective S1P agonist probes can be important tools to causally associate biological events with specific receptor-derived signals. We have identified, through systematic HTS and directed follow-up screening, a number of novel chemotypes of S1P₁ and S1P₃ selective agonists. Much greater numbers and more potent S1P₁ agonists were identified compared with S1P₃. We report, to our knowledge, the first S1P₃ agonist with selectivity against S1P₁. Through receptor modeling and ligand docking studies, we have characterized the difference between the receptor pockets and provide insights into the specific interactions that determine selectivity. These studies suggest that the diaryloxadiazole S1P₁ and dicyclohexylamide S1P₃ selective agonists interact primarily with the hydrophobic binding pocket and, in contrast to previously reported agonists, there are no obvious interactions with the glutamate and arginine residues characterizing the polar region of the binding site. Thus, our receptor structure models can aid in rational design and further optimization of selective ligands. The full agonist potential of the best compounds was characterized biologically by showing receptor internalization, protein phosphorylation, polyubiquitinylation, and calcium flux for S1P₁ and S1P₃, respectively. Analysis of the chemistry space characterizing the MLSMR and MBHF screening libraries and shape comparison of these libraries against the docked conformations of the selective agonists rationalize the observed greater hit rates and on average higher potency of the S1P₁ versus S1P₃ agonists.

METHODS

Materials. CHO-K1 CRE-bla, CHO-K1 NFAT-bla, and 5HT1A/ga16 CHO-K1 NFAT-bla cells lines, pcDNA3.1(+)-hygromycin, lipofectamine 2000, LiveBlazer dye, and all media components except serum were purchased from Invitrogen. pcDNA3-S1P₁, pcDNA3-S1P₂, and pcDNA3-S1P₃ were obtained from the Missouri S&T cDNA Resource Center (www.cdna.org). The ga16 gene was subcloned from pcDNA1 into pcDNA3.1(+)/hygromycin. Forskolin, probenecid, and fatty acid free BSA were purchased from Sigma. Fetal calf serum (FCS), bovine growth serum (BGS), and charcoal dextran stripped serum (CDS) were obtained from Hyclone. CA4 dye was purchased from Molecular Probes. BAS3430808 (**28**) was purchased from Asinex.

Cell Line Generation. CHO-K1 S1P₁/CRE-bla, CHO-K1 S1P₂/CRE-bla, and CHO-K1 S1P₃-ga16/NFAT-bla cell lines were generated by standard methods (20); cells were cultured in growth media (Dulbecco's modified Eagle's medium (DMEM), 10% heat-inactivated BGS, 0.1 mM nonessential amino acids (NEAA), 1 mM sodium pyruvate, 25 mM HEPES, 5 mM L-glutamine, 2 mg mL⁻¹ geneticin, and 1× penicillin–streptomycin. The media for S1P₃-ga16/NFAT-bla cell line also includes 200 μg mL⁻¹ hygromycin.

S1P₁ CRE-bla CHO Reporter Assay. Cells were suspended (0.3×10^6 mL⁻¹ in 384 well-format or 1.25×10^6 mL⁻¹ in 1536 well format) in phenol red free DMEM containing 0.5% charcoal/dextran treated FBS, 0.1 mM NEAA, 1 mM sodium pyruvate, 25 mM HEPES, and 5 mM L-glutamine. The assay began by dispensing 10 μL (4 μL for 1536 well format) of cell suspension to each well of the assay plates. The cells were then allowed to incubate in the plates for 20 h at 37 °C in 5% CO₂. Then test compound or controls were added by pintool, followed by forskolin (2 μM for 384 well format, 4 μM for 1536 well format). SEW2871 was added to 1 μM to positive control wells. Plates were then incubated at 37 °C in 5% CO₂ for 4 h. After the incubation, GeneBLAzer fluorescent substrate mixture, containing 15 mM probenecid, was added. After 2 h of incubation at RT in the dark, plates were read on an Envision (384 well format) or a ViewLux (1536 well format) plate reader.

CRE-bla Reporter Counterscreen Assays. Cells were suspended (0.3×10^6 mL⁻¹ for 384 well format or 1.25×10^6 mL⁻¹ for 1536 well format) in phenol red free DMEM containing 0.5% charcoal/dextran treated FBS, 0.1 mM NEAA, 1 mM sodium pyruvate, 25 mM HEPES, and 5 mM L-glutamine. The assay began by dispensing 10 μL (4 μL for 1536 well format) of cell suspension to each well of the assay plates. The cells were then allowed to incubate in the plates for 20 h at 37 °C in 5% CO₂. Then test compound or controls were added by pintool, followed by forskolin (2 μM for 384 well format, 4 μM for 1536 well format). SEW2871 was added to 1 μM to positive control wells. Plates were then incubated at 37 °C in 5% CO₂ for 4 h. After the incubation, GeneBLAzer fluorescent substrate mixture, containing 15 mM probenecid, was added. After 2 h of incubation at RT in the dark, plates were read on an Envision (384 well format) or a ViewLux (1536 well format) plate reader.

S1P₃-ga16-NFAT-bla Reporter Assay. Cells were suspended to a concentration of 1×10^6 mL⁻¹ in phenol red free DMEM containing 0.5% charcoal/dextran treated FBS, 0.1 mM NEAA, 1 mM sodium pyruvate, 25 mM HEPES, and 5 mM L-glutamine. The assay began by dispensing 5 μL of cell suspension to each test well of a 1536 well plate (10 μL for 384 well format). The plated cells were incubated overnight at 37 °C in 5% CO₂. Test compound or controls were added by pintool. The S1P positive control was also added to the appropriate control wells to a final concentration of 1 μM. Plates were then incubated at 37 °C in 5% CO₂ for 4 h. After the incubation, GeneBLAzer fluorescent substrate mixture, containing 15 mM probenecid, was added. After 2 h of incubation at RT in the dark, plates were read on an

Envision (384 well format) or a ViewLux (1536 well format) plate reader.

5HT1A/Gα16-NFAT-bla Reporter Counterscreen Assay. 5HT1A/ga16 CHO-K1 NFAT-bla cells were suspended to a concentration of 1×10^6 mL⁻¹ in phenol red free DMEM containing 2% charcoal/dextran treated FBS, 0.1 mM NEAA, 1 mM sodium pyruvate, 25 mM HEPES, and 5 mM L-glutamine. The assay began by dispensing 10 μL of cell suspension to each test well of a 384 well plate. The plated cells were incubated overnight at 37 °C in 5% CO₂. Test compound or controls were added by pintool. The 5-carboxamidotryptamine (5-CT) positive control was added to the positive control wells to a final concentration of 125 μM. Plates were then incubated at 37 °C in 5% CO₂ for 4 h. After the incubation, GeneBLAzer fluorescent substrate mixture, containing 15 mM probenecid, was added. After 2 h of incubation at RT in the dark, plates were read on an Envision plate reader.

Concentration–Response Curve Fitting. For each compound, percent activation was plotted against compound concentration and fitted to a four-parameter equation describing a sigmoidal concentration–response curve with adjustable baseline using Assay Explorer software by MDL. The reported EC₅₀ values are generated from fitted curves by solving for x-intercept at the 50% activity level of y-intercept. In cases where the highest concentration tested (45 μM) did not result in >50% inhibition or where no curve fit was achieved, the EC₅₀ was determined manually depending on the observed inhibition at the individual concentrations. Compounds with EC₅₀ values of greater than 10 μM were considered inactive, compounds with EC₅₀ equal to less than 10 μM are considered active.

PubChem Unique Assay Identifiers (AIDs) Associated with uHTS

Assay Results. Data associated with the reported results have been deposited into PubChem with the following AIDs: 449 and 1044, S1P₁ primary agonist and agonism potentiator assay for MLSMR and MBHF library, respectively; 466, 467, and 468, S1P₁ concentration–response data for potentiator, parental cell line, and agonist, respectively; 373, S1P₃ primary agonist assay; 439 and 1192, S1P₃ concentration–response and purchased analogs, respectively.

S1P₁ Secondary Assays. S1P₁–GFP internalization and ubiquitination Western blots were performed as previously described (22).

Intact cell S1P₁ phosphorylation. Phosphorylation experiments were carried out in monolayers of confluent stable 293-S1P₁–GFP cells grown in 6-well plates. Cells were washed twice with serum-free, phosphate-free DMEM and incubated in the same medium for 2 h prior to labeling with ³²P-orthophosphate (80 mCi mL⁻¹, 2 h). Following stimulation with the indicated agonists or vehicle control for 30 min at 37 °C, the monolayers were washed twice with ice-cold PBS and solubilized in radio immune precipitation assay (RIPA) buffer containing a cocktail of protease inhibitors (Roche) and 1 mM EDTA, 0.5 M glycerolphosphate, 1 mM phenylmethylsulfonyl fluoride, 1 μM Na₂VO₄, and 1 nM okadaic acid. After centrifugation (16,000 × g for 15 min), the supernatants were first equalized for protein content using the BCA method (Pierce) and subsequently immunoprecipitated with an anti-GFP antibody as previously reported (22). Following separation of the immunoprecipitated receptor by SDS-PAGE (4–12% gels), the gels were autoradiographed for 24 h at –80 °C, and the extent of ligand-stimulated S1P₁–GFP phosphorylation was compared with that of vehicle alone.

S1P₃ Calcium Flux Assay. S1P₃-ga16-NFAT-bla cells were plated in 25 μL of 0.5% CDS media at 12,500 cells well⁻¹ in 384 well Corning black clear bottom tissue culture treated plates. After brief centrifugation, CA4 dye, 25 μL, was added, and the cells incubated at 37 °C for 1 h. The calcium flux experiments were collected at 37 °C on a Molecular Devices Flexstation. Fluorescence intensity (485 nm excitation/510 nm emis-

sion) was collected every 2.5 s for 3 min. After a 30 s baseline collection, compound or S1P was added in quadruplicate. Calcium flux was evaluated as area under the curve for the first 60 s following agonist addition. Values are normalized to 1 μM S1P as 100% of control. The resulting 10 point concentration–response curves were fitted to a sigmoidal dose response with variable slope in Graph Pad Prism.

S1P₂ CRE-bla, S1P₂ TANGO, and S1P₃ TANGO Reporter Selectivity Assays. CHO-K1 S1P₂-CRE-bla cells were dispensed (10 μL of 1×10^6 cells mL^{-1}) to 384 well assay plates and incubated overnight at 37 °C in a humidified incubator. Test compounds, S1P, or vehicle only were dispensed to all wells. Plates were then incubated at 37 °C in 5% CO₂ for 4 h. After the incubation, 2.2 μL well⁻¹ GeneBLazer fluorescent substrate mixture (prepared according to the manufacturer's protocol and containing 15 mM probenecid) was added. After 2 h of incubation at RT in the dark, plates were read on the EnVision plate reader (PerkinElmer Lifesciences, Turku, Finland) at an excitation wavelength 405 nm and emission wavelengths of 590 and 460 nm. The S1P₄ and S1P₅ TANGO stable cell lines were obtained from Invitrogen and assayed according Invitrogen's protocol with 1 μM S1P as the positive control.

S1P₁ and S1P₁ L276F ERK Phosphorylation Assay. The L276F mutation was generated using the GeneTailor kit (Invitrogen) with pcDNA3-S1P₁ as the DNA template and the following oligonucleotides: S1P₁ L276F_F (5'-GCACCGCTCTTCATCCTGTTCTGC TGGATGTG-3') and S1P₁ L276F_R (5'-CAGGATGAAGAGCGGTGCC CAGCAGCGCAT-3'). The mutation was confirmed by sequencing. CHO-K1 cells were transfected overnight (Fugene, Roche) in 70% confluent 10 cm dishes with wild-type S1P₁ or L276 mutant S1P₁ DNA. Cells from each 10 cm dish were harvested and seeded into three 6-well plates in 10% FCS DMEM supplemented with 0.1% NEAA and sodium pyruvate and incubated overnight. The media was changed to DMEM for 5 h, and each well was treated with S1P or compound for 5 min. The wells were washed with ice-cold PBS, and cells were harvested by scraping the well in 1 mL lysis buffer (Cell Signaling). The samples were centrifuged and diluted 1:1 with sample diluent, and 100 μL of sample was added to wells of a phospho-ERK1/2 ELISA plate, incubated overnight, and washed. Wells were developed as described in the product manual. OD₄₅₀ values for each transfection were normalized to 100% of high control (1 μM S1P) and 0% of control (vehicle-treated wells).

S1P₁ and S1P₃ Receptor Structure Models. The initial model for the S1P₁ receptor was generated using the STRUFAST algorithm (28), a recent profile–profile alignment algorithm using convergent island statistics (29) to determine local alignment score significance. This algorithm is implemented in the TIP software system (30, 31). The high-resolution crystal structure of chain A of bovine rhodopsin (PDB 1u19, 2.2 Å resolution) (15) with retinal in the unactivated (cis) conformation was used as template, aligning residues 41–351 of S1P₁ to residues 34–349 of the rhodopsin template. This initial homology model was then optimized by repositioning the second extracellular loop connecting the TM4 and TM5 domains because of the absence of the template disulfide bridge connecting this loop with the TM3 domain and because this loop interferes with residues Arg120, Glu121, and Arg292 in S1P₁, which have been shown to be essential for binding of the natural S1P ligand (16). In the resulting structure, the transmembrane helices TM4, TM5, and TM7 and the connecting loop between TM4 and TM5 were independently optimized followed by a global minimization of the structure to 0.05 kcal mol⁻¹ Å⁻¹ root-mean-square gradient using the OPLS (optimized potential for liquid simulations) force field implemented in Schrödinger Macromodel (32). During the global minimization, the α -helix backbone atoms were frozen ± 1 Å to avoid local movements of the helices that was observed

otherwise; required rearrangement of the transmembrane helices associated with receptor activation make it plausible that the unactivated receptor is not in a globally minimized conformation. For comparison, we generated a model based on a more recent structure of lumirhodopsin (PDB 2hpy, 2.8 Å resolution) (24), a photoactivated all-trans retinal intermediate of the activated receptor. The model differs slightly in the middle of helix three and in the loop connecting TM4 and TM5; the side-chain-minimized models also differ in the orientation of the Glu121 and Arg120 residues, indicating that local structural movements in these areas may be associated with receptor activation. Previous S1P-receptor homology models were based on lower resolution or modeled rhodopsin structures (18, 19).

The final S1P₁ docking model was obtained by optimizing the binding pocket side chains by induced fit docking (IFD) (23) with S1P and FTY720-P (S-isomer) as ligands and using the default settings (other than indicated below). The IFD protocol is implemented in Schrödinger Maestro and includes a constraint receptor minimization step followed by initial flexible Glide docking of the ligands using a softened potential (reduced Coulomb van der Waals cutoff and scaling van der Waals radii to 0.5) to generate a diverse ensemble of potential poses. For each pose, the nearby receptor structure (using a cutoff of 4 Å) is refined using Prime (prediction of side chain orientation followed minimization in presence of the docked ligand). Each ligand is then redocked (using Glide) into its corresponding optimized low-energy receptor structure and ranked by GlideScore. Based on the established binding mode, two of the three (Arg120, Glu121, and Arg292) polar side chains known to interact with S1P were constraint as required hydrogen bonds during the IFD runs (16). The resulting receptor–ligand complexes were evaluated based on docking score, emodel energy, and Prime energies and visually to select the best and most abundant side-chain orientations among the IFD results.

The S1P₃ receptor model was then built based on the above S1P₁ structure template using the Prime comparative modeling module; both receptor structures were capped after their terminal secondary structure residues aligning S1P₁ Glu42–Met326 to S1P₃ Ser36–Val313 with identical positions of the backbone atoms except a gap of seven amino acids of S1P₃ in the loop connecting TM5 and TM6.

Agonist Docking. Docking was performed in Schrödinger Glide (33) using the above receptor structures of S1P₁ and S1P₃. A starting 3D conformation for the ligands was generated using the ChemAxon conformer plugin (34, 35); ligands (S1P, FTY720-P) were ionized at pH 7.4 using the pK_a plugin (36). In the case of S1P and FTY720-P (S-isomer), the Arg120 and Glu121 in S1P₁ and Arg114 and Glu115 in S1P₃ were constraint as hydrogen bond donors and acceptors, respectively. Up to 10 best poses per ligand were retained and analyzed by docking score and emodel energy and visually. The 1,3-diazole-1,2,4-oxadiazoles **5–8** were first docked flexibly into the S1P₁ receptor using Glide XP to better account for the hydrophobic interaction in the bottom part of the pocket. Poses that interacted with the repositioned loop (compare model development above) were removed, and the remaining poses were evaluated by Glide score and emodel energy and visually. The best pose was selected, and all structures were aligned to this pose followed by docking optimization of the so prepositioned ligands. Structures were ranked by glide score and emodel energy, and the most comparable poses are reported to visualize the binding mode in the S1P₁ receptor (Figure 6). These poses when scored against the S1P₃ receptor grid have Coulomb–vdW energies of 10,000 due to interaction with Phe263 (docking score 0). When docking the oxadiazole ligands flexibly into the S1P₃ receptor grid, we obtained poses that appear less favorable after evaluating docking energies and visual inspection; for example, the

diethoxyphenyl moiety points toward the polar region of the pocket and does not interact in the hydrophobic region or the ligands are structurally distorted. A pose of oxadiazole **6** that was obtained is provided in Supplementary Figure S8; the orientation of the ligand is rotated around the axis of the three aromatic rings (to avoid interaction with the Phe263 residue), and the pyridyl aromatic plane appears almost perpendicular to the oxadiazole; although the diethoxyphenyl moiety does not align well with the corresponding S1P₁ orientation, one of the ethoxy residues still interacts in the hydrophobic region. The S1P₃-selective dicyclohexylamide structures **20** and **28** were docked flexibly into the S1P₃ receptor using Glide XP. The poses in which the dicyclohexylamide moieties align best were selected and, with the cyclohexyl substituent in an equatorial position, were minimized using the OLPS force field followed by docking optimization in the receptor grid. The best poses are reported (Figure 7). When these poses are evaluated in the S1P₁ receptor grid, they are invalid (by Coulomb–vdW, docking score 0). When ligands are docked flexibly into the S1P₁ receptor, all obtained poses have different orientations and in none of the poses did the dicyclohexylamide moieties of the two ligands align in the hydrophobic part of the binding pocket (in particular, the cyclohexyl moieties of **20** would not interact in the hydrophobic pocket). When the S1P₃ pose of **28** is optimized in the S1P₁ receptor, the ligand is rotated so that the aromatic (furyl-oxadiazole) plane orients between the TM6 and TM3 domains, parallel to the corresponding aryl moiety of the S1P₁ diaryloxadiazole ligands (Supplementary Figure S9).

All visualizations were prepared in PyMOL (37).

Receptor binding site volumes were calculated in MOE (38); the receptor site volumes differ by ~50–100 Å³ when measured inside a box around the diaryloxadiazole compounds (1780 vs 1727 Å³ to 1953 vs 1864 Å³); the S1P₃ pocket is contracted by 1.5–1.8 Å compared with S1P₁ (as measured point to point between S1P₁ Leu276–Glu121 and S1P₃ Phe263–Glu115).

Library Comparison. The MLSMR (~60,000 at the time of screening) and Maybridge HitFinder (MBHF, 16,000 diverse structures) libraries were compared using a cell-based and a fingerprint-based approach. Extended connectivity fingerprints (ECFP6) and Tanimoto similarities were calculated in Scitegic Pipeline Pilot (39). Neighborhood statistics show that the majority of each library is less similar than 0.4 to the other (Supplementary Figure S2). An optimized six-dimensional BCUTS (40) chemistry space for the combined libraries using the standard 3D hydrogen-suppressed descriptors was generated using Diverse Solutions (41). Diversity analysis using six bins per dimension (6⁶ cells) shows an overlap of 0.68 and 0.52, respectively, and a cell-based Tanimoto index of 0.42. To illustrate global library diversity (Supplementary Figure S3) and the diversity of hits for S1P₁ and S1P₃ (Figures 1 and 2) an optimized two-dimensional chemistry space was used. The chemistry space density/occupancy was calculated as the sum of structures falling into each cell (Supplementary Figure S11).

Cluster and Similarity Analysis of Active Series. A total of 508 compounds with EC₅₀ results for S1P₁ were hierarchically clustered using Leadscape (21) keys and a cluster height of 0.6. For each cluster, Z-scores (defined as the number of standard deviations that the mean of each cluster is away from the mean of the entire data set) were calculated based on pEC₅₀ values of the agonist, potentiator, and parental assays. Clusters and singletons with activity in the parental (CHO CRE BLA) cell line or high activity in another GPCR β-lactamase reporter assay (5HT1A) were removed for likely unspecific effects. Structures with reactive or undesired structural features were also removed. A similar procedure was used to identify the active series of the S1P₃ agonist assay. The Z-scores based on the primary assay results (Supplementary Table S2) illustrate that the

clusters are derived from only the most active compounds confirmed in a concentration–response assay. They also indicate selectivity where initial concentration–response data was not available for both receptors. To follow-up the most interesting series and develop initial SAR, structures with S1P₁ EC₅₀ ≤ 1 μM (in the initial HTS concentration–response assay) were selected as seeds, and 80% similar structures were added from the entire library. The resulting compounds were hierarchically clustered with a cutoff threshold of 0.7. Selected examples of the retested 3,5-diaryl-1,2,4-oxadiazole series are given in Table 1. The most active representatives are summarized in Supplementary Table S3. To follow up on S1P₃, compounds with an EC₅₀ < 10 μM were selected as seeds, and in addition to the 80% similarity expansion, structures with >60% similarity to the 5-(2,2-diphenylethyl)-3,4-pyridyl-oxadiazole **16** were added because of the much smaller number of actives and generally lower activities. One series of 5-sulfanyl-cyano-tetrahydroisoquinolines was removed entirely.

Shape-Based Comparison. A 3D conformer library (10 Mio structures) was generated from the combined MLSMR and HitFinder library using Omega (42) from Open Eye (43). Shape similarities (44) of this 3D conformer library were generated against the best docking poses of the S1P₃-selective dicyclohexylamide **20** and the S1P₁-selective diaryl-oxadiazole **6** using Open Eye ROCS and the largest ShapeTanimoto for each query structure of the library was used to plot the number of shape-similar compounds as a function of similarity cutoff (Supplementary Figure S10).

Acknowledgment: This work was supported by the National Institutes of Health Molecular Library Screening Center Network Grant U54 MH074404-01 and by grants from NIAID to H.R. We thank Pierre Baillargeon for compound management and Kashif Hoda for data management with PubChem.

Supporting Information Available: This material is free of charge via the Internet.

REFERENCES

1. Sanna, M. G., Liao, J., Jo, E., Alfonso, C., Ahn, M. Y., Peterson, M. S., Webb, B., Lefebvre, S., Chun, J., Gray, N., and Rosen, H. (2004) Sphingosine 1-phosphate (S1P) receptor subtypes S1P1 and S1P3, respectively, regulate lymphocyte recirculation and heart rate, *J. Biol. Chem.* **279**, 13839–13848.
2. Forrest, M., Sun, S. Y., Hajdu, R., Bergstrom, J., Card, D., Doherty, G., Hale, J., Keohane, C., Meyers, C., Milligan, J., Mills, S., Nomura, N., Rosen, H., Rosenbach, M., Shei, G. J., Singer, I. I., Tian, M., West, S., White, V., Xie, J., Proia, R. L., and Mandala, S. (2004) Immune cell regulation and cardiovascular effects of sphingosine 1-phosphate receptor agonists in rodents are mediated via distinct receptor subtypes, *J. Pharmacol. Exp. Ther.* **309**, 758–768.
3. Wei, S. H., Rosen, H., Matheu, M. P., Sanna, M. G., Wang, S. K., Jo, E., Wong, C. H., Parker, I., and Cahalan, M. D. (2005) Sphingosine 1-phosphate type 1 receptor agonism inhibits transendothelial migration of medullary T cells to lymphatic sinuses, *Nat. Immunol.* **6**, 1228–1235.
4. Jo, E., Sanna, M. G., Gonzalez-Cabrera, P. J., Thangada, S., Tigyi, G., Osborne, D. A., Hla, T., Parrill, A. L., and Rosen, H. (2005) S1P1-selective *in vivo*-active agonists from high-throughput screening: off-the-shelf chemical probes of receptor interactions, signaling, and fate, *Chem. Biol.* **12**, 703–715.
5. Alfonso, C., McHeyzer-Williams, M. G., and Rosen, H. (2006) CD69 down-modulation and inhibition of thymic egress by short- and long-term selective chemical agonism of sphingosine 1-phosphate receptors, *Eur. J. Immunol.* **36**, 149–159.
6. Sanchez, T., and Hla, T. (2004) Structural and functional characteristics of S1P receptors, *J. Cell. Biochem.* **92**, 913–922.

7. Hla, T. (2003) Signaling and biological actions of sphingosine 1-phosphate, *Pharmacol. Res.* **47**, 401–407.
8. Mandala, S., Hajdu, R., Bergstrom, J., Quackenbush, E., Xie, J., Milligan, J., Thornton, R., Shei, G. J., Card, D., Keohane, C., Rosenbach, M., Hale, J., Lynch, C. L., Rupprecht, K., Parsons, W., and Rosen, H. (2002) Alteration of lymphocyte trafficking by sphingosine-1-phosphate receptor agonists, *Science* **296**, 346–349.
9. Brinkmann, V., Davis, M. D., Heise, C. E., Albert, R., Cottens, S., Hof, R., Bruns, C., Prieschl, E., Baumruker, T., Hiestand, P., Foster, C. A., Zollinger, M., and Lynch, K. R. (2002) The immune modulator FY720 targets sphingosine 1-phosphate receptors, *J. Biol. Chem.* **277**, 21453–21457.
10. Niessen, F., Schaffner, F., Furlan-Freguia, C., Pawlinski, R., Bhattacharjee, G., Chun, J., Derian, C. K., Andrade-Gordon, P., Rosen, H., and Ruf, W. Dendritic cell PAR1-S1P3 signalling couples coagulation and inflammation, *Nature* **452**, 654–658.
11. Rosen, H. (2005) Chemical approaches to the lysophospholipid receptors, *Prostaglandins Other Lipid Mediators* **77**, 179–184.
12. Rosen, H., and Liao, J. (2003) Sphingosine 1-phosphate pathway therapeutics: a lipid ligand-receptor paradigm, *Curr. Opin. Chem. Biol.* **7**, 461–468.
13. Sanna, M. G., Wang, S. K., Gonzalez-Cabrera, P. J., Don, A., Marsolais, D., Matheu, M. P., Wei, S. H., Parker, I., Jo, E., Cheng, W. C., Cahalan, M. D., Wong, C. H., and Rosen, H. (2006) Enhancement of capillary leakage and restoration of lymphocyte egress by a chiral S1P1 antagonist *in vivo*, *Nat. Chem. Biol.* **2**, 434–441.
14. Palczewski, K., Kumasaka, T., Hori, T., Behnke, C. A., Motoshima, H., Fox, B. A., Le Trong, I., Teller, D. C., Okada, T., Stenkamp, R. E., Yamamoto, M., and Miyano, M. (2000) Crystal structure of rhodopsin: a G protein-coupled receptor, *Science* **289**, 739–745.
15. Okada, T., Sugihara, M., Bondar, A. N., Elstner, M., Entel, P., and Buss, V. (2004) The retinal conformation and its environment in rhodopsin in light of a new 2.2 Å crystal structure, *J. Mol. Biol.* **342**, 571–583.
16. Parrill, A. L., Wang, D., Bautista, D. L., Van Brocklyn, J. R., Lorincz, Z., Fischer, D. J., Baker, D. L., Liliom, K., Spiegel, S., and Tigyi, G. (2000) Identification of Edg1 receptor residues that recognize sphingosine 1-phosphate, *J. Biol. Chem.* **275**, 39379–39384.
17. Inagaki, Y., Pham, T. T., Fujiwara, Y., Kohno, T., Osborne, D. A., Igarashi, Y., Tigyi, G., and Parrill, A. L. (2005) Sphingosine 1-phosphate analogue recognition and selectivity at S1P4 within the endothelial differentiation gene family of receptors, *Biochem. J.* **389**, 187–195.
18. Deng, Q., Clemas, J. A., Chrebet, G., Fischer, P., Hale, J. J., Li, Z., Mills, S. G., Bergstrom, J., Mandala, S., Mosley, R., and Parent, S. A. (2007) Identification of Leu276 of the S1P1 receptor and Phe263 of the S1P3 receptor in interaction with receptor specific agonists by molecular modeling, site-directed mutagenesis, and affinity studies, *Mol. Pharmacol.* **71**, 724–735.
19. Fujiwara, Y., Osborne, D. A., Walker, M. D., Wang, D. A., Bautista, D. A., Liliom, K., Van Brocklyn, J. R., Parrill, A. L., and Tigyi, G. (2007) Identification of the hydrophobic ligand binding pocket of the S1P1 receptor, *J. Biol. Chem.* **282**, 2374–2385.
20. Kunapuli, P., Ransom, R., Murphy, K. L., Pettibone, D., Kerby, J., Grimwood, S., Zuck, P., Hodder, P., Lacson, R., Hoffman, I., Inglese, J., and Strulovici, B. (2003) Development of an intact cell reporter gene beta-lactamase assay for G protein-coupled receptors for high-throughput screening, *Anal. Biochem.* **314**, 16–29.
21. *Leadscope Enterprise*; Leadscope Inc.: Columbus, OH, 2007.
22. Gonzalez-Cabrera, P. J., Hla, T., and Rosen, H. (2007) Mapping pathways downstream of sphingosine 1-phosphate subtype 1 by differential chemical perturbation and proteomics, *J. Biol. Chem.* **282**, 7254–7264.
23. Sherman, W., Day, T., Jacobson, M. P., Friesner, R. A., and Fasid, R. (2006) Novel procedure for modeling ligand/receptor induced fit effects, *J. Med. Chem.* **49**, 534–553.
24. Nakamichi, H., and Okada, T. (2006) Local peptide movement in the photoreaction intermediate of rhodopsin, *Proc. Natl. Acad. Sci. U.S.A.* **103**, 12729–12734.
25. Zhang, Y., Devries, M. E., and Skolnick, J. (2006) Structure modeling of all identified G protein-coupled receptors in the human genome, *PLoS Comput. Biol.* **2**, e13.
26. Pham, T.-C. T., Fells, J. I., Osborne, D. A., North, E. J., Naor, M. M., and Parrill, A. L. (2008) Molecular recognition in the sphingosine 1-phosphate receptor family, *J. Mol. Graphics Modell.* **26**, 1189–1201.
27. Vachal, P., Toth, L. M., Hale, J. J., Yan, L., Mills, S. G., Chrebet, G. L., Keohane, C. A., Hajdu, R., Milligan, J. A., Rosenbach, M. J., and Mandala, S. (2006) Highly selective and potent agonists of sphingosine-1-phosphate 1 (S1P1) receptor, *Bioorg. Med. Chem. Lett.* **16**, 3684–3687.
28. Debe, D. A., Danzer, J. F., Goddard, W. A., and Poleksic, A. (2006) STRUCTFAST: protein sequence remote homology detection and alignment using novel dynamic programming and profile-profile scoring, *Proteins* **64**, 960–967.
29. Poleksic, A., Danzer, J. F., Hambly, K., and Debe, D. A. (2005) Convergent Island Statistics: a fast method for determining local alignment score significance, *Bioinformatics* **21**, 2827–2831.
30. Hambly, K., Danzer, J., Muskal, S., and Debe, D. A. (2006) Interrogating the druggable genome with structural informatics, *Mol. Divers.* **10**, 273–281.
31. *TIP*; Eidogen-Sertanty Inc: San Diego, CA, 2007.
32. *Macromodel*; Schrödinger LLC: Portland, OR, 2007.
33. *Glide*; Schrödinger, LLC: Portland, OR, 2007.
34. Imre, G., Kalászi, A., Jákli, I., and Farkas, Ö. Advanced Automatic Generation of 3D Molecular Structures, presented at the 1st European Chemistry Congress, Budapest, Hungary, 2006.
35. ChemAxon, Budapest, Hungary, (2006) .
36. Szegezdi, J., and Csizmadia, F. A method for calculating the pK_a values of small and large molecules, presented at the American Chemical Society Spring Meeting, Chicago, IL, 2007.
37. DeLano, W. L. *PyMOL*; DeLano Scientific LLC: Palo Alto, CA, 2007.
38. *Molecular Operating Environment*; Chemical Computing Group Inc.: Montreal, Canada, 2007.
39. *Pipeline Pilot*; Accelrys: San Diego, CA, 2007.
40. Pearlman, R. S., and Smith, K. M. (1998) Novel software tools for chemical diversity, *Perspect. Drug Discovery Des.* **9–11**, 339–353.
41. *Diverse Solutions*; Tripos: St. Louis, MO, 2005.
42. Bostrom, J. (2001) Reproducing the conformations of protein-bound ligands: a critical evaluation of several popular conformational searching tools, *J. Comput.-Aided Mol. Des.* **15**, 1137–1152.
43. Open Eye Scientific Software, Inc., Santa Fe, NM, (2007) .
44. Grant, J. A., Gallardo, M. A., and Pickup, B. T. (1996) A fast method of molecular shape comparison: a simple application of a Gaussian description of molecular shape, *J. Comput. Chem.* **17**, 1653–1666.